Solid State Ionics 346 (2020) 115218

Contents lists available at ScienceDirect

Solid State Ionics

journal homepage: www.elsevier.com/locate/ssi

Phase compositions, structures and properties of scandia-stabilized zirconia solid solution crystals co-doped with yttria or ytterbia and grown by directional melt crystallization

D.A. Agarkov[a,b,c,*], M.A. Borik[c], S.I. Bredikhin[a,b,c], I.N. Burmistrov[a,b,c], G.M. Eliseeva[a,c], A.V. Kulebyakin[c], I.E. Kuritsyna[a,c], E.E. Lomonova[c], F.O. Milovich[d], V.A. Myzina[c], N.Yu. Tabachkova[c,d]

[a] Institute of Solid State Physics RAS, Academician Osip'yan str., 2, 142432 Chernogolovka, Moscow District, Russia
[b] Moscow Institute of Physics and Technology, Institutskiy lane 9, 141701 Dolgoprudny, Moscow District, Russia
[c] Prokhorov General Physics Institute RAS, Vavilov str. 38, 119991 Moscow, Russia
[d] National University of Science and Technology (MISIS), Leninskiy prospect, 4, 119049 Moscow, Russia

ARTICLE INFO

Keywords:
Skull melting
Growth from melt
Scandia-stabilized zirconia
Dielectric materials
Solid electrolytes

ABSTRACT

The effect of co-doping an impurity on the transport parameters and cubic phase stabilization of ZrO_2–Sc_2O_3-based solid solutions has been compared for Y_2O_3 and Yb_2O_3 dopants. Solid solution crystals of $(ZrO_2)_{1-x-y}(Sc_2O_3)_x(Yb_2O_3)_y$ and $(ZrO_2)_{1-x-y}(Sc_2O_3)_x(Y_2O_3)_y$ (x = 0.08–0.10, y = 0.01, 0.02) were grown by directional melt crystallization in a cold crucible. Co-doping of the $(ZrO_2)_{1-x}(Sc_2O_3)_x$ crystals (x = 0.08–0.10) with 2 mol% Y_2O_3 or Yb_2O_3 for all experimental compositions produced transparent homogeneous single crystals of the t" phase or the cubic phase. For co-doping of the scandia-stabilized zirconia crystals with 1 mol% Y_2O_3 or Yb_2O_3, the stabilization of the high-temperature phases depended on the Sc_2O_3 content in the solid solutions. For co-doping of the solid solutions with 1 mol% Y_2O_3 or Yb_2O_3, the conductivity of the crystals increased with the Sc_2O_3 concentration. For co-doping of the crystals with 2 mol% Y_2O_3 or Yb_2O_3, the conductivity decreased with the Sc_2O_3 concentration. At scandia concentrations of 9–10 mol%, the high-temperature conductivity of the crystals co-doped with ytterbia were higher compared to those with yttria co-doping. The $(ZrO_2)_{0.9}(Sc_2O_3)_{0.09}(Yb_2O_3)_{0.01}$ crystals had the highest conductivity over the entire experimental temperature range.

1. Introduction

Materials based on ZrO_2–Sc_2O_3 solid solutions used in solid oxide fuel cells (SOFCs) are of great interest because they have the highest ionic conductivity among zirconia-based solid electrolytes [1–4]. However, there are problems with compounds having the highest conductivity, i.e., ZrO_2 – (9–11) mol% Sc_2O_3, when used as materials for electrolytic membranes; these problems are unstable transport characteristics at operating temperatures and a transformation of a rhombohedral phase to a cubic phase during heating. Stabilizing the highly conductive cubic phase is one of the possible ways to solve these problems by co-doping ZrO_2 – Sc_2O_3 solid solutions with yttria or rare-earth element oxides [5–10]. The choice of co-doped impurities is dictated by the necessity to obtain a single-phase cubic solid solution stable in the range from room temperature to operating temperatures (700–1000 °C) and to maintain the high conductivity typical of the ZrO_2–Sc_2O_3 system. Efficient impurities that stabilize the high-temperature cubic phase are yttria and ytterbia [9,11–16]. In particular, a recently published article [17] conducted a detailed study on the effect of 1 mol% Yb_2O_3 co-doping on the metastable tetragonal phases present in 8–9 mol% Sc_2O_3–ZrO_2. X-ray diffraction (XRD), transmission electron microscopy (TEM) and Raman spectroscopy analysis confirmed the metastable t′ phase in $8Sc_2O_3$–$92ZrO_2$ and t″ phase in $9Sc_2O_3$–$91ZrO_2$.

It is well known that the phase composition and properties of solid electrolytes depend significantly on the material synthesis technique that is used [18]. For example, the phase composition of molten materials may differ significantly from the phase composition of materials synthesized at low temperatures. In this work, we synthesized the materials by directional melt crystallization in a cold crucible. This method was used earlier for synthesizing crystals of a wide range of

* Corresponding author at: Institute of Solid State Physics RAS, Academician Osip'yan str., 2, 142432 Chernogolovka, Moscow District, Russia.
E-mail address: agarkov@issp.ac.ru (D.A. Agarkov).

https://doi.org/10.1016/j.ssi.2019.115218
Received 20 July 2019; Received in revised form 13 December 2019; Accepted 30 December 2019

solid electrolytes [19–22].

The aim of this work is to synthesize ZrO_2–Sc_2O_3 solid solution crystals co-doped with yttria or ytterbia to study their transport properties and to compare the effect of the impurities (Y_2O_3 or Yb_2O_3) on the transport parameters and cubic phase stabilization of ZrO_2–Sc_2O_3-based solid solutions.

2. Experimental

$(ZrO_2)_{1-x-y}(Sc_2O_3)_x(Yb_2O_3)_y$ and $(ZrO_2)_{1-x-y}(Sc_2O_3)_x(Y_2O_3)_y$ solid solution crystals (x = 0.08–0.10, y = 0.01, 0.02) were grown using directional melt crystallization in a cold crucible [23]. The crystals were grown in a Kristall-407 unit (frequency 5.28 MHz, maximum output power 60 kW). The raw materials were zirconia, scandia and ytterbia powders of at least 88.88% purity. A mixture of the powders in the required weight ratio was placed in a crucible (120 mm in diameter) that contained a set of water-cooled copper tubes. To start the melting process, we added 5–10 g of Zr metal into the powder. Directional melt crystallization was achieved by moving the melt container down relative to the inductor at a 10 mm/h speed. The weight of the melt was 5–6 kg. After switching off the growth unit, the melt was cooled in the crucible to room temperature. The temperature of the ingot surface was recorded with a Gulton 900–1999 radiation pyrometer in a 2000–1000 °C range and a Pt/Pt-Rh thermocouple in the 1000–500 °C range; the ingot cooling rates in these temperature ranges were ~200 °C/min and ~30 °C/min, respectively. The melt crystallized to an ingot consisting of discrete crystals that could be mechanically separated from one another after ingot cooling.

The chemical composition of the as-grown crystals was studied using a JEOL 5910 LV scanning electron microscope with an INCA energy dispersion unit. Molten zirconia, scandia, yttria, and ytterbia were used as references for the crystal composition study. The structure of the crystals was studied using X-ray diffraction (Bruker D8, Germany) with a standard method used for single crystals. For the X-ray study, the crystals were cut into plates perpendicular to the ⟨100⟩ direction. The phase composition of the crystals was also studied using Raman scattering spectroscopy (Renishaw inVia Raman spectrometer). The excitation source was a 532 nm laser. The instrument for Raman study of the crystals at room temperature and at operating temperatures of up to 1000 °C was described in detail earlier [24–26].

Transmission electron microscopy (TEM) was carried out using a JEM 2100 (Jeol, Japan) microscope at an acceleration voltage of 200 keV. An ultrasonic disc cutter was used to cut samples into discs 3 mm in diameter, which were then polished to a thickness of ~100 μm. The discs were further dimpled to a thickness of ~25 μm in a dimple grinder and then ion-milled in a precision ion polishing system (Gatan, PIPS II).

The conductivity of the zirconia base crystals was studied in a 400–900 °C range with a Solartron SI 1260 frequency analyser over a 1 Hz – 5 MHz frequency range with a 24 mV AC current amplitude. The test plates had an area of 7 × 7 mm^2 each and were 0.5 mm in thickness. The current contacts were produced on the reverse side of the crystals by burning in a platinum paste at 950 °C for 1 h in air. The impedance spectra were processed with ZView (ver. 2.8) (Scribner Associates, Inc., USA) software. The specific conductivity of the crystals was calculated from the impedance spectrum processing results, while taking into account the specimen dimensions.

3. Results and discussion

Table 1 shows the compositions of the solid solutions, their brief notations used hereafter, and the phase composition and lattice parameters of the crystals.

The as-grown crystals had columnar shapes that were typical of crystals grown by crystallization in a cold crucible. The transverse dimension of the crystals was 20 mm, with a length of 30–50 mm (Fig. 1).

Analysis of the appearance of the crystals provides initial information on their phase composition, i.e., whether a crystal is single-phase or contains multiple phases. The presence of multiple phases or structural defects may cause light scattering at defects or phase boundaries, making the crystal opalescent or semitransparent.

The 8Sc1YSZ crystals were almost completely inhomogeneous and semitransparent, and only the top parts that formed at the end of crystallization had some small transparent regions (Fig. 1a). At higher Sc_2O_3 concentrations in the solid solutions (9 mol%), 9Sc1YSZ, the crystals had transparent regions in the bottom parts of the 9Sc1YSZ crystals forming at an early crystallization stage and semitransparent (opaque) regions in the top parts of the crystal (end of crystallization). Some 9Sc1YSZ crystals exhibited interchanging transparent and opaque regions in the middle parts of the as-crystallized melt ingots (Fig. 1b). Transparent single crystals without visible defects containing 1 mol% Y_2O_3 were only obtained at a 10 mol% Sc_2O_3 concentration (Fig. 1c). All the crystals doped with 2 mol% Y_2O_3 (8Sc2YSZ, 9Sc2YSZ, and 10Sc2YSZ) were homogeneous and transparent single crystals.

The appearance of the crystals stabilized with 1 mol% Yb_2O_3 differed from that of the crystals stabilized with 1 mol% Y_2O_3. The 8Sc1YbSZ crystals were homogeneous and opaque, without visible defects (Fig. 1d). The 9Sc1YbSZ crystals, unlike the 9Sc1YSZ crystals, were transparent and homogeneous single crystals (Fig. 1e). At higher Sc_2O_3 concentrations in the solid solutions (10 mol%, 10Sc1YbSZ), the crystals were opalescent and contained microcracks in the bulk (Fig. 1f). Doping with 2 mol% Yb_2O_3, by analogy with 2 mol% Y_2O_3 doping, produced transparent and homogeneous single crystals.

The phase composition of the crystals additionally doped with 1 mol % Y_2O_3 changed with an increase in the Sc_2O_3 concentration. The phase composition of the 8Sc1YSZ crystals was inhomogeneous along the ingot length. Most of the 8Sc1YSZ crystal volume contained the tetragonal ZrO_2 modification ($c/\sqrt{2}a$ ~1.005), and only the top parts of the crystals contained a mixture of cubic and tetragonal phases. The 9Sc1YSZ crystals were two-phase and contained regions with tetragonal and cubic structures. The 10Sc1YSZ crystals were single-phase and had a cubic fluorite structure. The 8Sc2YbSZ, 9Sc2YbSZ, and 10Sc2YbSZ crystals were single-phase cubic single crystals. The lattice parameters of the crystals stabilized with 2 mol% Y_2O_3 decreased monotonically with an increase in the Sc_2O_3 concentration.

The phase compositions of the crystals additionally doped with 1 mol% Yb_2O_3 also changed with an increase in the Sc_2O_3 concentration. The 8Sc1YbSZ crystals were homogeneous and tetragonal ($c/\sqrt{2}a$ ~1.005). The 9Sc1YbSZ crystals were single-phase cubic crystals, while the 10Sc1YbSZ crystals contained two phases, i.e., the cubic and rhombohedral zirconia modifications. The 8Sc2YSZ, 9Sc2YSZ, and 10Sc2YSZ crystals were single-phase cubic single crystals. The lattice parameters of the crystals stabilized with 2 mol% Yb_2O_3, and by analogy the crystals stabilized by doping with 2 mol% Y_2O_3, decreased with an increase in the Sc_2O_3 concentration in the crystals.

For example, Fig. 2 shows typical diffraction patterns of the 8Sc1YbSZ and 9Sc1YbSZ crystals for the surfaces of plates cut perpendicular to the ⟨100⟩ direction.

Thus, co-doping of the $(ZrO_2)_{1-x}(Sc_2O_3)_x$ crystals (x = 0.08–0.10) with 2 mol% Y_2O_3 or Yb_2O_3 produced homogeneous transparent crystals with a fluorite structure. At a co-doping impurity (Y_2O_3 or Yb_2O_3) concentration of 1 mol%, the phase compositions of the crystals depended on the Sc_2O_3 concentration. The high-temperature cubic phase of the Sc1YSZ crystals stabilized at a total stabilizing oxide concentration of 11 mol%, whereas for the Sc1YbSZ crystals, the stabilization occurred at a total stabilizing oxide concentration of 10 mol%. Despite the smaller ionic radius of Yb^{3+} compared with that of Y^{3+}, the cubic phase stabilized in crystals co-doped with Yb_2O_3 at lower Sc_2O_3 concentrations in the solid solution than for crystals co-doped with Y_2O_3.

In binary ZrO_2-R_2O_3 systems, a decrease in the ionic radius reduces the temperature of the transition from the high-temperature cubic phase to the low-temperature tetragonal phase, leading to the

Table 1
Composition, notation, phase composition and lattice parameters of the $(ZrO_2)_{1-x-y}(Sc_2O_3)_x(Yb_2O_3)_y$ and $(ZrO_2)_{1-x-y}(Sc_2O_3)_x(Y_2O_3)_y$ crystals.

Composition	Specimen	Phase composition	Lattice parameter	
			a, nm	*c*, nm
$(ZrO_2)_{1-x-y}(Sc_2O_3)_x(Y_2O_3)_y$				
$(ZrO_2)_{0.91}(Sc_2O_3)_{0.08}(Y_2O_3)_{0.01}$	8Sc1YSZ	t′	0.3600(1)	0.5119(2)
		c	0.5103(1)	
$(ZrO_2)_{0.90}(Sc_2O_3)_{0.08}(Y_2O_3)_{0.02}$	8Sc2YSZ	c	0.5101(1)	
$(ZrO_2)_{0.90}(Sc_2O_3)_{0.09}(Y_2O_3)_{0.01}$	9Sc1YSZ	t′	0.3601(1)	0.5109(2)
		c	0.5095(1)	
$(ZrO_2)_{0.89}(Sc_2O_3)_{0.09}(Y_2O_3)_{0.02}$	9Sc2YSZ	c	0.5098(1)	
$(ZrO_2)_{0.89}(Sc_2O_3)_{0.10}(Y_2O_3)_{0.01}$	10Sc1YSZ	c	0.5093(1)	
$(ZrO_2)_{0.88}(Sc_2O_3)_{0.10}(Y_2O_3)_{0.02}$	10Sc2YSZ	c	0.5096(1)	
$(ZrO_2)_{1-x-y}(Sc_2O_3)_x(Yb_2O_3)_y$				
$(ZrO_2)_{0.91}(Sc_2O_3)_{0.08}(Yb_2O_3)_{0.01}$	8Sc1YbSZ	t′	0.3598(1)	0.5113(2)
$(ZrO_2)_{0.90}(Sc_2O_3)_{0.08}(Yb_2O_3)_{0.02}$	8Sc2YbSZ	c	0.5099(1)	
$(ZrO_2)_{0.90}(Sc_2O_3)_{0.09}(Yb_2O_3)_{0.01}$	9Sc1YbSZ	c	0.5094(1)	
$(ZrO_2)_{0.89}(Sc_2O_3)_{0.09}(Yb_2O_3)_{0.02}$	9Sc2YbSZ	c	0.5096(1)	
$(ZrO_2)_{0.89}(Sc_2O_3)_{0.10}(Yb_2O_3)_{0.01}$	10Sc1YbSZ	c	0.5095(1)	
		r	0.3563(2)	0.9003(2)
$(ZrO_2)_{0.88}(Sc_2O_3)_{0.10}(Yb_2O_3)_{0.02}$	10Sc2YbSZ	c	0.5095(1)	

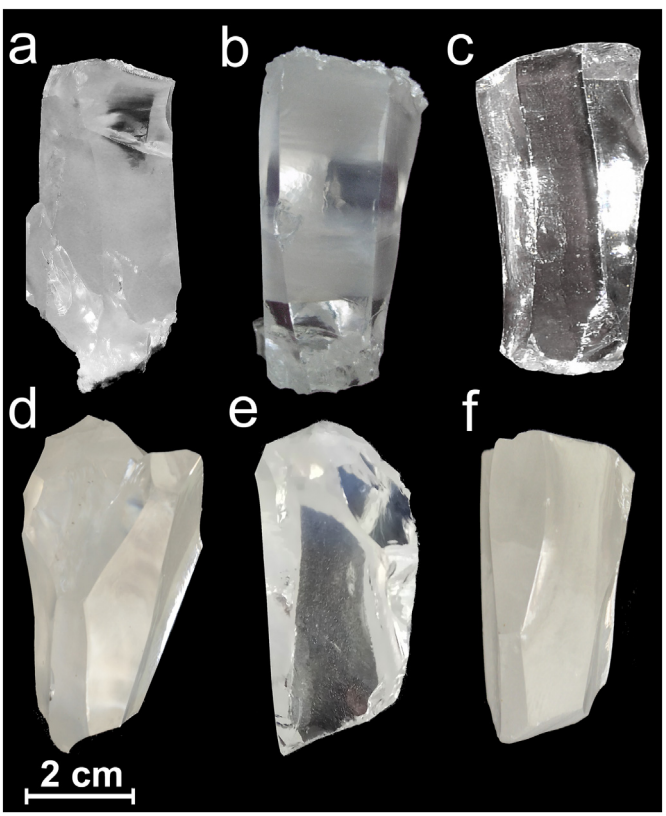

Fig. 1. Appearance of the (a) 8Sc1YSZ, (b) 9Sc1YSZ, (c) 10Sc1YSZ, (d) 8Sc1YbSZ, (e) 9Sc1YbSZ and (f) 10Sc1YbSZ crystals.

preservation of a high-temperature cubic phase at room temperature for low stabilizing oxide concentrations. This regularity may also hold for the studied ternary systems.

The phase compositions of the crystals were also studied using Raman spectroscopy. Fig. 3 shows the Raman spectra of the test crystals. The Raman spectra of the 8Sc1YSZ and 8Sc1YbSZ crystals contained peaks typical of the tetragonal phase [27,28]. In the Raman spectra of the 9Sc1YSZ crystals, the peaks were broadened due to the presence of the cubic and tetragonal phases in the crystals. The Raman spectra of the 10Sc1YbSZ crystals contained peaks that were also broadened and corresponded to the rhombohedral phase [28], which was possibly due to the presence of the cubic phase in these crystals.

The Raman spectra of the 10Sc1YSZ, 8Sc2YSZ, 9Sc2YSZ, 9Sc1YbSZ and 8Sc2YbSZ crystals were similar and contained, along with the cubic phase peaks, a 480 cm^{-1} peak that had been reported to correspond to the tetragonal t″ phase [29–31]. This phase had a tetragonality degree of $c/\sqrt{2}a = 1$ but belonged to the $P4_2/nmc$ space symmetry group due to the shift of the oxygen ions in the anion sublattice [30]. Raman spectra typical of the t-ZrO_2, t″- ZrO_2 and c-ZrO_2 phases were reported earlier [32]. Thus, the structure of these crystals identified as cubic using X-ray diffraction were the tetragonal t″ phase, as indicated by Raman spectroscopy. Only the spectra of the 10Sc2YSZ, 9Sc2YbSZ, and 10Sc2YbSZ crystals corresponded to the cubic phase.

Fig. 4 shows the TEM images and the corresponding selected area electron diffraction (SAED) patterns for the 8Sc1YbSZ and 9Sc1YbSZ crystals. The TEM images of the 8Sc1YbSZ crystal (Fig. 4a) showed a twinning structure that was typical of the t' phase [1]. Similar TEM images were also obtained for other crystals that contained the tetragonal phase. The twins formed during single crystal cooling as a result of the cubic-to-tetragonal transition in accordance with the ZrO_2–Sc_2O_3 phase diagram. The presence of these defects changed the optical transparency of the crystals due to light scattering at twin boundaries. The 9Sc1YbSZ crystals (Fig. 4b) did not contain twins. The bright-field image was typical of single-phase cubic crystals. However, the SAED patterns of the 9Sc1YbSZ crystals contained reflections that were impossible for the perfect fluorite type structure but were allowed for a tetragonal structure. The presence of the 110- and 112-type reflections suggested ordered shifting of the oxygen atoms and hence a distortion of the *Fm3m* space group symmetry. Thus, the data suggested that the crystalline structure of the 9Sc1YbSZ crystals corresponded to the structure of the tetragonal t″ phase.

Similar TEM images and the corresponding SAED patterns were also observed for the 10Sc1YSZ, 8Sc2YSZ, 9Sc2YSZ, and 8Sc2YbSZ crystals. These data also agreed with the Raman data for the crystals.

Typical impedance spectra for crystals with different phase compositions are shown in Fig. 5. The 8Sc1YSZ and 9Sc1YSZ were two-phase crystals (t + c); the 10Sc1YbSZ crystal was also a two-phase crystal (c + r); 8Sc1YbSZ was single-phase (t); and 9Sc1YbSZ and 10Sc1YSZ were single-phase (c). Despite the different phase compositions of the crystals, their impedance spectra had no fundamental differences. These spectra exhibited arcs in their high-frequency portions, which corresponded to bulk conductivity, as well as low-frequency arcs, which characterized the polarization resistance of the electrodes. There were no intermediate arcs corresponding to grain boundary conductivity. One could therefore assume that the twin and phase

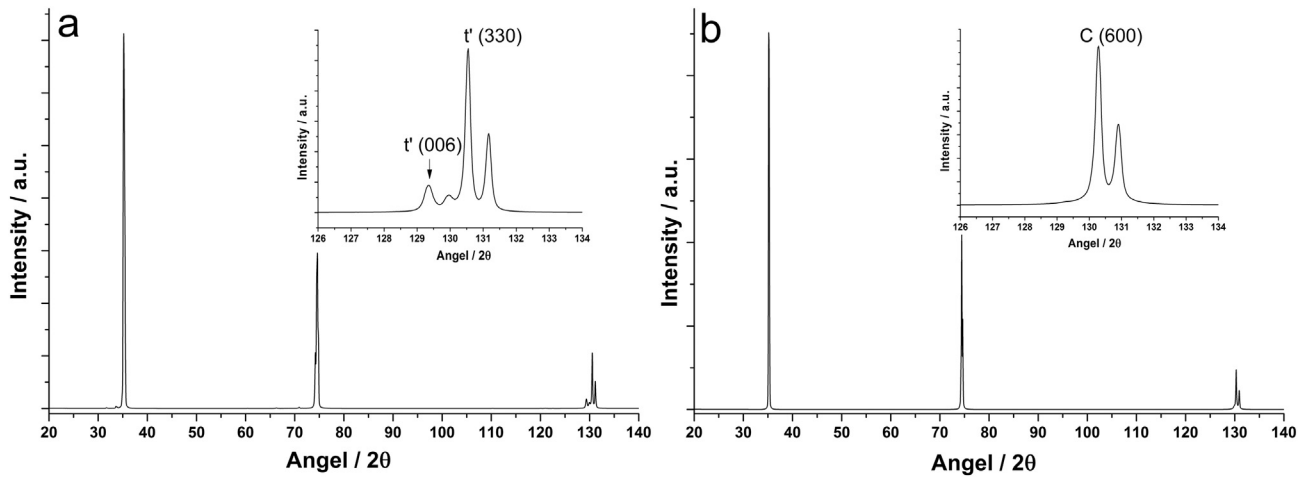

Fig. 2. Diffraction patterns of the (a) 8Sc1YbSZ and (b) 9Sc1YbSZ crystals for the surfaces of plates cut perpendicular to the ⟨100⟩ direction.

boundaries did not contribute to the total conductivity of the crystals.

Fig. 6 shows the specific conductivity of the crystals as a function of temperature in Arrhenius coordinates. It could be seen from the specific conductivity vs. temperature curves that only the curve of the 10Sc1YbSZ crystal had a bend in the 450–550 °C range caused by the rhombohedral-to-cubic phase transition. The 10Sc1YSZ crystals had the highest conductivity among all the $(ZrO_2)_{1-x-y}(Sc_2O_3)_x(Y_2O_3)_y$ crystals in the entire experimental temperature range, and the 9Sc1YbSZ crystals had the highest conductivity for the $(ZrO_2)_{1-x-y}(Sc_2O_3)_x(Yb_2O_3)_y$ crystal series.

Fig. 7 shows the conductivity of the ScYbSZ and ScYSZ crystals as a function of the Sc_2O_3 content.

Fig. 7 suggested that the conductivity of the crystals increased with the Sc_2O_3 content in the crystals co-doped with 1 mol% Y_2O_3 or Yb_2O_3. The conductivity of the crystals co-doped with 2 mol% Y_2O_3 or Yb_2O_3 decreased with an increase in the Sc_2O_3 concentration. For comparable Sc_2O_3 and stabilizing oxide concentrations, the conductivity of the crystals co-doped with Yb_2O_3 was always higher than that of the crystals co-doped with Y_2O_3. The patterns of the experimental conductivity vs. concentration curves could be accounted for by taking into account the specimen phase composition data. The conductivities of the single-phase tetragonal 8Sc1YbSZ and 8Sc1YSZ crystals and those of the two-phase 9Sc1YSZ crystal, which were a mixture of the tetragonal and cubic phases, were close at approximately 0.1 S/cm. The 9Sc1YbSZ crystals, which were single-phase pseudocubic crystals (the t″ phase), had the highest conductivity. At a Sc_2O_3 concentration of 10 mol% (the 10Sc1YbSZ specimen), the crystals had rhombohedral phase regions, and their conductivity decreased. The 10Sc1YSZ crystals were also single-phase pseudocubic crystals (the t″ phase), but their conductivity was lower than that of the 9Sc1YbSZ crystals that had a similar crystalline structure. This difference in the conductivity could be attributed to the larger ionic radius of Y^{3+} compared with that of Yb^{3+}. The introduction of a larger ion in the case of a heterovalent substitution increases lattice stress and thus reduces the conductivity. Furthermore, the 10Sc1YSZ and 9Sc1YbSZ crystals had different stabilizing oxide concentrations (11 and 10 mol%, respectively). An increase in the total stabilizing oxide concentration to above a threshold level, which depends on the type of stabilizing impurity, reduces the conductivity of the crystals due to the formation of oxygen + ion clusters [33]. The conductivity of the single-phase cubic crystals stabilized with 2 mol% Y_2O_3 or Yb_2O_3 decreased with an increase in the total stabilizing oxide concentration. At a stabilizing oxide concentration of 2 mol%, the crystals with a total concentration of 10 mol%, i.e., 8Sc2YSZ and 8Sc2YbSZ, had the highest conductivity.

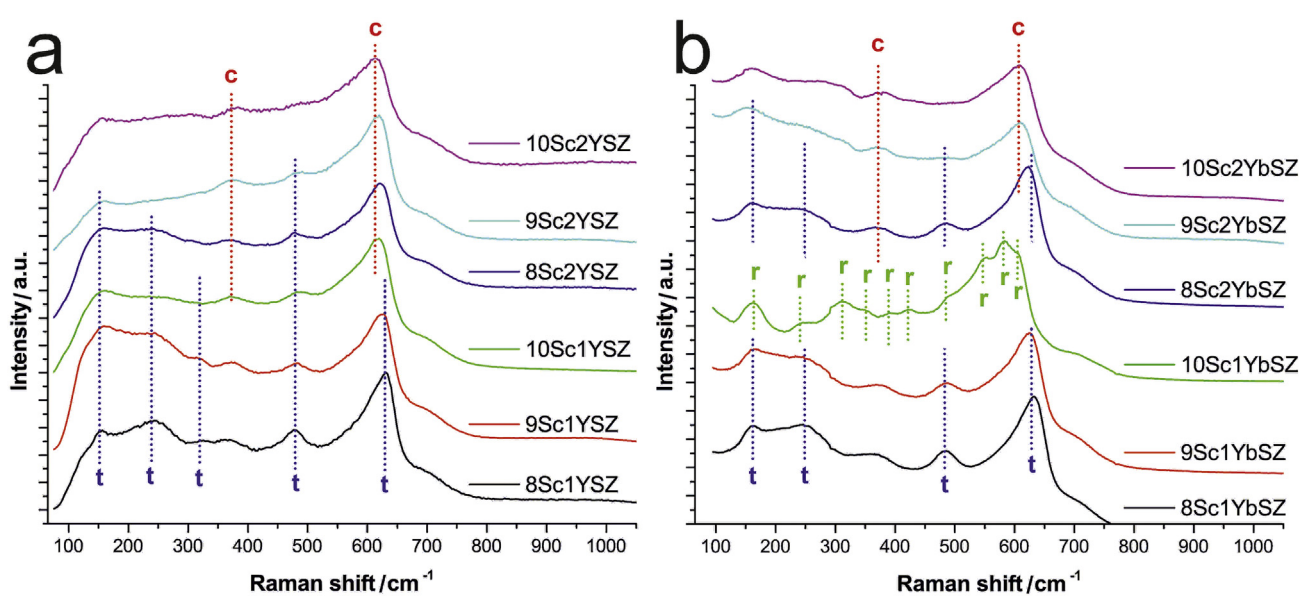

Fig. 3. Raman spectra of the (a) $(ZrO_2)_{1-x}(Sc_2O_3)_x(Y_2O_3)_y$ and (b) $(ZrO_2)_{1-x}(Sc_2O_3)_x(Yb_2O_3)_y$ crystals.

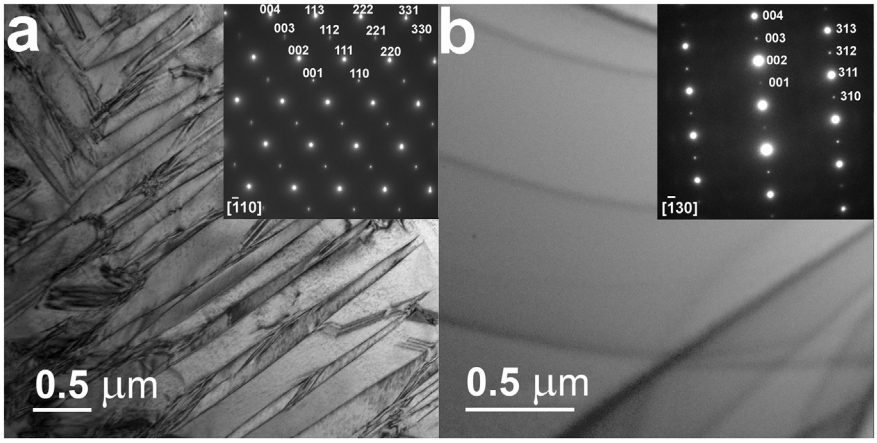

Fig. 4. TEM images of the (a) 8Sc1YbSZ and (b) 9Sc1YbSZ crystals. Insets show selected area electron diffraction patterns.

4. Conclusions

We compared the phase composition and transport properties of the $(ZrO_2)_{1-x-y}$ $(Sc_2O_3)_x(Yb_2O_3)_y$ and $(ZrO_2)_{1-x-y}(Sc_2O_3)_x(Y_2O_3)_y$ solid solution crystals (x = 0.08–0.10, y = 0.01, 0.02) grown by directional melt crystallization in a cold crucible.

We show that the stabilization of the pseudocubic t″ phase as a result of co-doping with scandia-stabilized zirconia with 1 mol% Y_2O_3 occurs at a total stabilizing oxide concentration of 11 mol%, whereas the cubic fluorite structure stabilizes at 12 mol%. The stabilization of

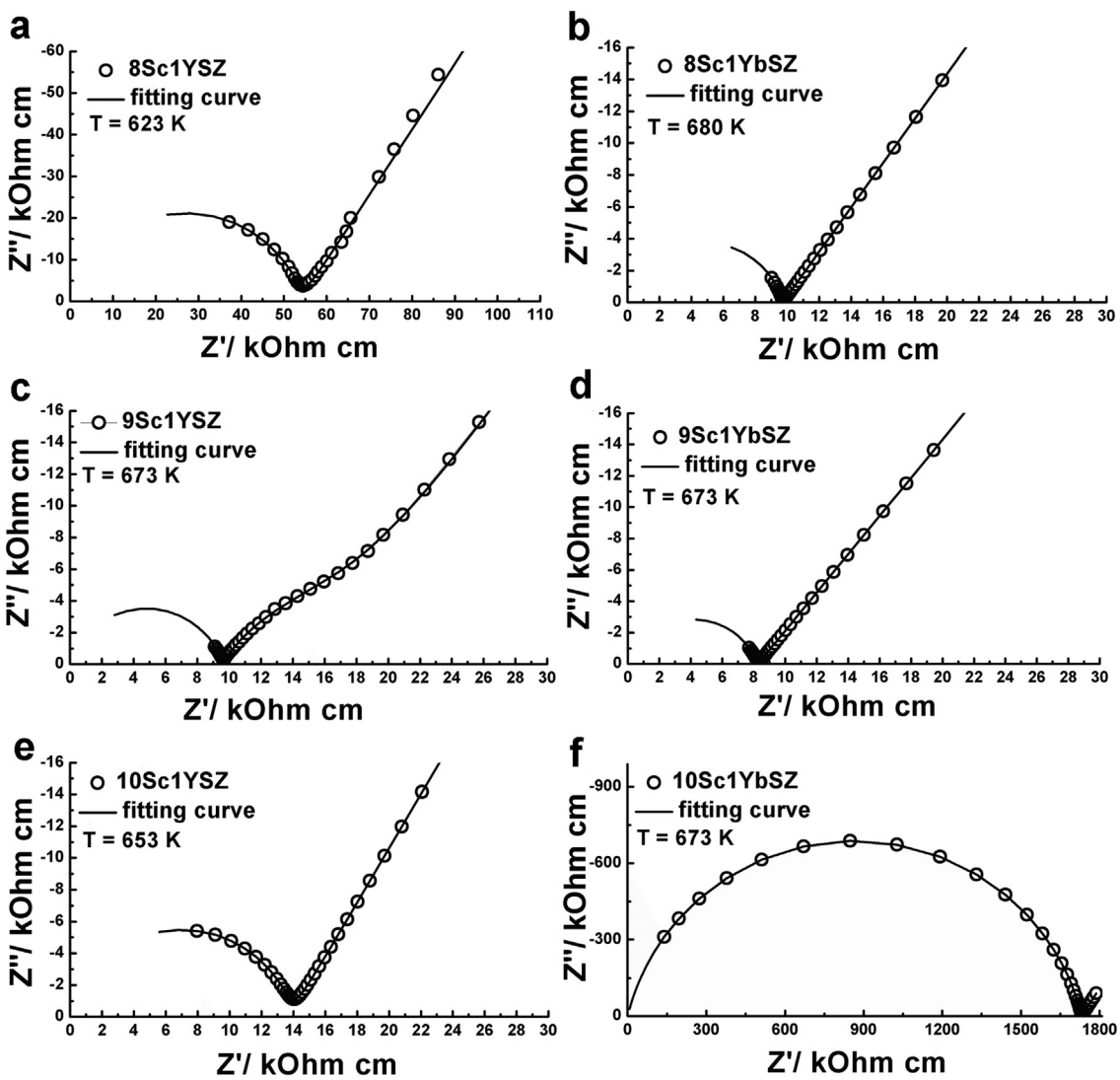

Fig. 5. Impedance spectra of the (a) 8Sc1YSZ, (b) 9Sc1YSZ, (c) 10Sc1YSZ, (d) 8Sc1YbSZ, (e) 9Sc1YbSZ and (f) 10Sc1YbSZ crystals.

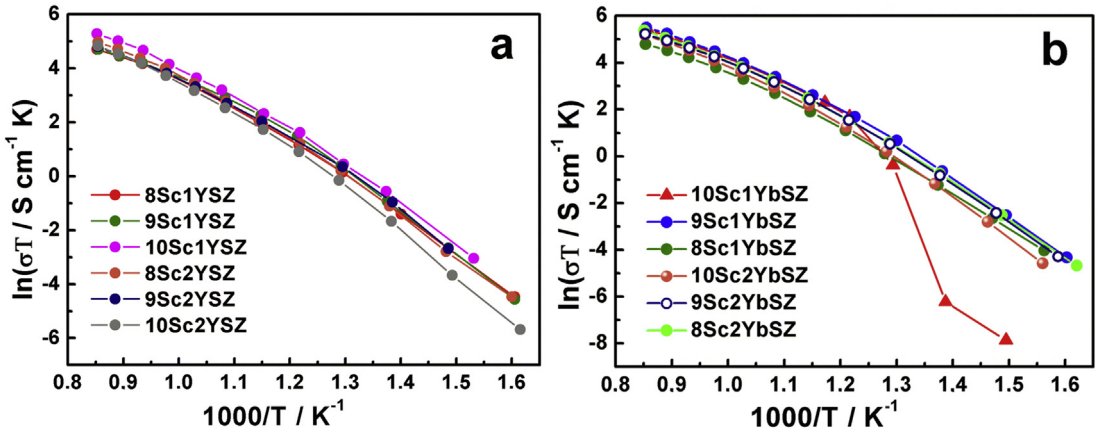

Fig. 6. Specific conductivity of the (a) $(ZrO_2)_{1-x}(Sc_2O_3)_x(Y_2O_3)_y$ and (b) $(ZrO_2)_{1-x}(Sc_2O_3)_x(Yb_2O_3)_y$ crystals as a function of temperature.

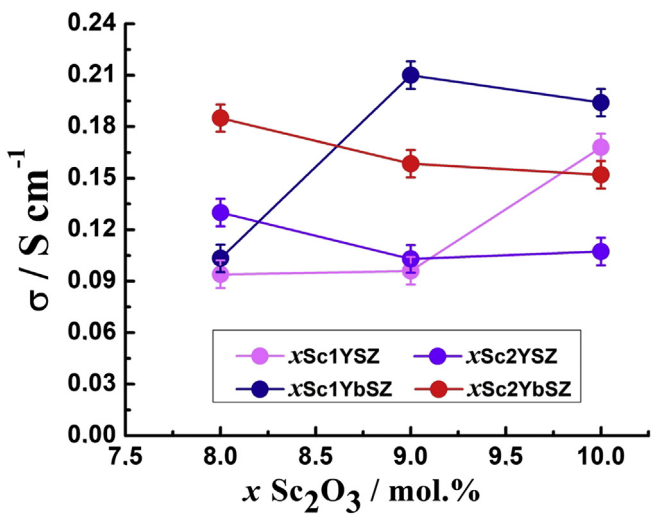

Fig. 7. Ionic conductivity at 900 °C of the $(ZrO_2)_{1-x}(Sc_2O_3)_x(Y_2O_3)_y$ and $(ZrO_2)_{1-x}(Sc_2O_3)_x(Yb_2O_3)_y$ crystals as a function of Sc_2O_3 content.

the high-temperature phases as a result of co-doping with 2 mol% Yb_2O_3 occurs at lower Sc_2O_3 concentrations in the solid solutions than when co-doping with 1 mol% Y_2O_3. The pseudocubic t″ phase in $(ZrO_2)_{0.99-x}(Sc_2O_3)_x(Yb_2O_3)_{0.01}$ stabilizes at a total stabilizing oxide concentration of 10 mol%, whereas the cubic fluorite structure stabilizes at 11 mol%. Co-doping of the $(ZrO_2)_{1-x}(Sc_2O_3)_x$ (x = 0.08–0.10) crystals with 2 mol% Y_2O_3 or Yb_2O_3 for all the experimental compositions produce transparent and homogeneous t″ phase or cubic phase single crystals.

We show that for co-doping of the solid solutions with 1 mol% Y_2O_3 or Yb_2O_3, the conductivity of the crystals increases with Sc_2O_3 concentration. For co-doping with 2 mol% Y_2O_3 or Yb_2O_3, the conductivity decreases with Sc_2O_3 concentration. The highest conductivities of the crystals co-doped with Y_2O_3 or Yb_2O_3 are observed at different Sc_2O_3 contents (10 and 9 mol%, respectively). At Sc_2O_3 contents of 9–10 mol %, the high-temperature conductivity of the crystals co-doped with Yb_2O_3 is higher than that of the crystals co-doped with Y_2O_3. The 9Sc1YbSZ crystals have the highest conductivity over the entire experimental temperature range.

CRediT authorship contribution statement

D.A. Agarkov: Data curation, Investigation, Writing - review & editing. **M.A. Borik:** Methodology, Writing - original draft. **S.I. Bredikhin:** Supervision, Methodology. **I.N. Burmistrov:** Data curation, Investigation. **G.M. Eliseeva:** Data curation, Investigation. **A.V. Kulebyakin:** Data curation, Investigation. **I.E. Kuritsyna:** Data curation, Investigation. **E.E. Lomonova:** Supervision, Methodology. **F.O. Milovich:** Data curation, Investigation. **V.A. Myzina:** Funding acquisition, Resources. **N.Yu. Tabachkova:** Project administration, Writing - original draft.

Declaration of competing interest

This statement is to certify that

- All authors have participated in (a) conception and design, or analysis and interpretation of the data; (b) drafting the article or revising it critically for important intellectual content; and (c) approval of the final version.
- This manuscript has not been submitted to, nor is under review at, another journal or other publishing venue.
- The authors have no affiliation with any organization with a direct or indirect financial interest in the subject matter discussed in the manuscript.
- The following authors have affiliations with organizations with direct or indirect financial interest in the subject matter discussed in the manuscript:

D.A. Agarkov (Institute of Solid State Physics RAS, Moscow Institute of Physics and Technology, Prokhorov General Physics Institute RAS).

M.A. Borik (Prokhorov General Physics Institute RAS).

S.I. Bredikhin (Institute of Solid State Physics RAS, Moscow Institute of Physics and Technology, Prokhorov General Physics Institute RAS).

I.N. Burmistrov (Institute of Solid State Physics RAS, Moscow Institute of Physics and Technology, Prokhorov General Physics Institute RAS).

G.M. Eliseeva (Institute of Solid State Physics RAS, Prokhorov General Physics Institute RAS).

A.V. Kulebyakin (Prokhorov General Physics Institute RAS).

I.E. Kuritsyna (Institute of Solid State Physics RAS, Prokhorov General Physics Institute RAS).

E.E. Lomonova (Prokhorov General Physics Institute RAS).

F.O. Milovich (National University of Science and Technology (MISIS).

V.A. Myzina (Prokhorov General Physics Institute RAS).

N.Yu. Tabachkova (Prokhorov General Physics Institute RAS, National University of Science and Technology (MISIS).

Acknowledgements

This work was performed with the financial support of the Russian Science Foundation (RSF), Projects 17-79-30071 and 19-72-10113. The synthesis and the study of the structure and transport properties of the $(ZrO_2)_{1-x}(Sc_2O_3)_x(Y_2O_3)_y$ crystals were supported with Grant 17-79-30071. The synthesis and the study of the structure and transport properties of the $(ZrO_2)_{1-x}(Sc_2O_3)_x(Yb_2O_3)_y$ crystals were supported with Grant 19-72-10113.

References

[1] S.P.S. Badwal, F.T. Ciacchi, D. Milosevic, Scandia-zirconia electrolytes for intermediate temperature solid oxide fuel cell operation, Solid State Ionics 136–137 (2000) 91–99, https://doi.org/10.1016/S0167-2738(00)00356-8.

[2] A. Kumar, A. Jaiswal, M. Sanbui, S. Omar, Oxygen-ion conduction in scandia-stabilized zirconia-ceria solid electrolyte ($(Sc2O3)_x$–$(CeO2)_1$–$(ZrO_2)_{99-x}$, $5 \le x \le 11$), J. Am. Ceram. Soc. 100 (2017) 659–668, https://doi.org/10.1111/jace.14595.

[3] D.W. Stricker, W.G. Carlson, Electrical conductivity in the ZrO2-rich region of several M2O3-ZrO2 system, J. Am. Ceram. Soc. 48 (1965) 286–289, https://doi.org/10.1111/j.1151-2916.1965.tb14742.x.

[4] M.A. Borik, S.I. Bredikhin, A.V. Kulebyakin, I.E. Kuritsyna, E.E. Lomonova, F.O. Milovich, V.A. Myzina, V.V. Osiko, V.A. Panov, P.A. Ryabochkina, S.V. Seryakov, N.Y. Tabachkova, Melt growth, structure and properties of (ZrO2)1-x (Sc2O3)x solid solution crystals (x = 0.035–0.11), J. Cryst. Growth 443 (2016) 54–61, https://doi.org/10.1016/j.jcrysgro.2016.03.004.

[5] H. Yamamura, T. Matsusita, H. Nishino, K. Kakinuma, Co-doping effect on electrical conductivity in the fluorite-type solid-solution systems Zr0.7(Sc1-xMx)0.3O2-δ (M = Ca, Mg, Al, Gd, Yb), J. Mater. Sci. Mater. Electron. 13 (2002) 57–61, https://doi.org/10.1023/A:1013643305260.

[6] D.S. Lee, W.S. Kim, S.H. Choi, J. Kim, H.-W. Lee, J.H. Lee, Characterization of ZrO2 co-doped with Sc2O3 and CeO2 electrolyte for the application of intermediate temperature SOFCs, Solid State Ionics 176 (2005) 33–39, https://doi.org/10.1016/j.ssi.2004.07.013.

[7] S. Omar, W.B. Najib, W. Chen, N. Bonanos, Electrical conductivity of 10 mol% Sc2O3–1 mol% M2O3–ZrO2 ceramics, J. Am. Ceram. Soc. 95 (2012) 1965–1972, https://doi.org/10.1111/j.1551-2916.2012.05126.x.

[8] R. Chiba, T. Ishii, F. Yoshimura, Temperature dependence of ionic conductivity in (1 − x) ZrO2 − (x − y)Sc2O3 − yYb2O3 electrolyte material, Solid State Ionics 91 (1996) 249–256, https://doi.org/10.1016/S0167-2738(96)83026-8.

[9] A. Spirin, V. Ivanov, A. Nikonov, A. Lipilin, S. Paranin, V. Khrustov, A. Spirina, Scandia-stabilized zirconia doped with yttria: synthesis, properties, and ageing behavior, Solid State Ionics 225 (2012) 448–452, https://doi.org/10.1016/j.ssi.2012.02.022.

[10] S. Omar, N. Bonanos, Ionic conductivity ageing behaviour of 10 mol.% Sc2O3 − 1 mol.% CeO2 − ZrO2 ceramics, J. Mater. Sci. 45 (2010) 6406–6410, https://doi.org/10.1007/s10853-010- 4723-x.

[11] V.V. Lakshmi, R. Bauri, Phase formation and ionic conductivity studies on ytterbiacodopedscandia stabilized zirconia (0.9ZrO2–0.09Sc2O3–0.01Yb2O3) electrolyte for SOFCs, Solid State Sci. 13 (2011) 1520–1525, https://doi.org/10.1016/j.solidstatesciences.2011.05.014.

[12] F. Yuan, J. Wang, H. Miao, C. Guo, W.G. Wang, Investigation of the crystal structure and ionic conductivity in the ternary system (Yb2O3)*x*–(Sc2O3, 0.11_*x*)–(ZrO2)0.89 (*x* = 0–0.11), J. Alloys Compd. 549 (2013) 200–205, https://doi.org/10.1016/j.jallcom.2012.09.089.

[13] A. Yamaji, T. Koshikawa, W. Araki, T. Adachi, Stabilization of a zirconia system and evaluation of its electrolyte characteristics for a fuel cell: based on electrical and mechanical considerations, J. Eng. Mater. Technol. 131 (2008) 011010–011016, https://doi.org/10.1115/1.3026557.

[14] V. Shukla, K. Balani, A. Subramaniam, S. Omar, Phase stability and conductivity in the pseudo ternary system of xYb2O3–(12–*x*)Sc2O3–88ZrO2 (0 ≤ x ≤ 5), Solid State Ionics 332 (2019) 93–101, https://doi.org/10.1016/j.ssi.2019.01.005.

[15] V. Shukla, A. Kumar, I.L. Basheer, K. Balani, A. Subramaniam, S. Omar, Structural characteristics and electrical conductivity of spark plasma sintered ytterbia co-doped Scandia stabilized zirconia, J. Am. Ceram. Soc. 100 (2017) 204–214, https://doi.org/10.1111/jace.14545.

[16] T.I. Politova, J.T.S. Irvine, Investigation of scandia–yttria–zirconia system as an electrolyte material for intermediate temperature fuel cells—influence of yttria content in system $(Y_2O_3)_x(Sc_2O_{3,\ 11-x})(ZrO_2)_{89}$, Solid State Ionics 168 (2004) 153–165, https://doi.org/10.1016/j.ssi.2004.02.007.

[17] V. Shukla, K. Balani, A. Subramaniam, S. Omar, Effect of thermal aging on the phase stability of $1Yb_2O_3$–xSc_2O_3–(99–x)ZrO2 (x = 7, 8 mol%), J. Phys. Chem. C 123 (2019) 21982–21992, https://doi.org/10.1021/acs.jpcc.9b05672.

[18] S. Hui, J. Roller, S. Yick, X. Zhang, C. Decès-Petit, Y. Xie, R. Maric, D. Ghosh, A brief review of the ionic conductivity enhancement for selected oxide electrolytes, J. Power Sources 172 (2007) 493–502, https://doi.org/10.1016/j.jpowsour.2007.07.071.

[19] S. Berendts, M. Lerch, Growth and characterization of low yttria–doped fully cubic stabilized zirconia-based single crystals, J. Cryst. Growth 371 (2013) 28–33, https://doi.org/10.1016/j.jcrysgro.2013.01.045.

[20] I. Valov, V. Ruhrup, R. Klein, T.-C. Rödel, A. Stork, S. Berendts, M. Dogan, H.-D. Wiemhöfer, M. Lerch, J. Janek, Ionic and electronic conductivity of nitrogen–doped ysz single crystals, Solid State Ionics 180 (2009) 1463–1470, https://doi.org/10.1016/j.ssi.2009.09.003.

[21] J.-P. Eufinger, M. Daniels, K. Schmale, S. Berendts, G. Ulbrich, M. Lerch, H.-D. Wiemhöfer, J. Janek, The model case of an oxygen storage catalyst – non-stoichiometry, point defects and electrical conductivity of single crystalline CeO2–ZrO2–Y2O3 solid solutions, Phys. Chem. Chem. Phys. (46) (2014) 25583–25600, https://doi.org/10.1039/C4CP03704A.

[22] M.A. Borik, S.I. Bredikhin, V.T. Bublik, A.V. Kulebyakin, I.E. Kuritsyna, E.E. Lomonova, F.O. Milovich, V.A. Myzina, V.V. Osiko, P.A. Ryabochkina, N.Y. Tabachkova, Structure and conductivity of yttria and scandia doped zirconia crystals grown by skull melting, J. Am. Ceram. Soc. 100 (2017) 5536–5547, https://doi.org/10.1111/jace.15074.

[23] V.V. Osiko, M.A. Borik, E.E. Lomonova, Synthesis of refractory materials by skull melting, Springer Hand Book of Crystal Growth, Springer, New York, 2010, pp. 433–477, , https://doi.org/10.1007/978-3-540-74761-1_14.

[24] D.A. Agarkov, I.N. Burmistrov, F.M. Tsybrov, I.I. Tartakovskii, V.V. Kharton, S.I. Bredikhin, In situ Raman spectroscopy analysis of the interfaces between Ni-based SOFC anodes and stabilized zirconia electrolyte, Solid State Ionics 302 (2017) 133, https://doi.org/10.1016/j.ssi.2016.12.034.

[25] D.A. Agarkov, I.N. Burmistrov, F.M. Tsybrov, I.I. Tartakovskii, V.V. Kharton, S.I. Bredikhin, Kinetics of NiO reduction and morphological changes in composite anodes of solid oxide fuel cells: estimate using Raman scattering technique, Russ. J. Electrochem. 52 (2016) 600, https://doi.org/10.1134/S1023193516070028.

[26] D.A. Agarkov, I.N. Burmistrov, F.M. Tsybrov, I.I. Tartakovskii, V.V. Kharton, S.I. Bredikhin, V.V. Kveder, Analysis of interfacial processes at the SOFC electrodes by in situ Raman spectroscopy, ECS Trans. 68 (2015) 2093, https://doi.org/10.1149/06801.2093ecst.

[27] H. Fujimori, M. Yashima, M. Kakihana, M. Yoshimura, Structural changes of scandia-doped zirconia solid solutions: Rietveld analysis and Raman scattering, J. Am. Ceram. Soc. 81 (1998) 2885, https://doi.org/10.1111/j.1151-2916.1998.tb02710.x.

[28] H. Fujimori, M. Yashima, M. Kakihana, M. Yoshimura, β-Cubic phase transition of scandia-doped zirconia solid solution: calorimetry, X-ray diffraction, and Raman scattering, J. Appl. Phys. 91 (2002) 6493, https://doi.org/10.1063/1.1471576.

[29] M. Yashima, S. Sasaki, M. Kakihana, Y. Yamaguchi, H. Arashi, M. Yoshimura, Oxygen-induced structural change of the tetragonal phase around the tetragonal-cubic phase-boundary in ZrO_2-$YO_{1.5}$ solid-solutions, Acta Crystallogr. Sect. B: Struct. Sci. 50 (1994) 663, https://doi.org/10.1107/S0108768194006257.

[30] M. Yashima, K. Ohtake, M. Kakihana, H. Arashi, M. Yoshimura, Determination of tetragonal-cubic phase boundary of $Zr_{1-x}R_xO_{2-x/2}$ (R = Nd, Sm, Y, Er and Yb) by Raman scattering, J. Phys. Chem. Solids 57 (1996) 17, https://doi.org/10.1016/0022-3697(95)00085-2.

[31] D.M. Lipkin, J.A. Krogstad, Y. Gao, C.A. Johnson, W.A. Nelson, C.G. Levi, Phase evolution upon ageing of air plasma spray t`-zirconia coatings: I - synchrotron X-ray diffraction, J. Am. Ceram. Soc. 96 (2013) 290, https://doi.org/10.1111/j.1551-2916.2012.05451.x.

[32] Y. Hemberger, N. Wichtner, C. Berthold, K.G. Nickel, Quantification of yttria in stabilized zirconia by Raman spectroscopy, Int. J. Appl. Ceram. Technol. 13 (2016) 116, https://doi.org/10.1111/ijac.12434.

[33] Y. Arachi, H. Sakai, O. Yamamoto, Y. Takeda, N. Imanishai, Electrical conductivity of the ZrO_2 –Ln_2O_3 (Ln-lanthanides) system, Solid State Ionics 121 (1999) 133, https://doi.org/10.1016/S0167-2738(98)00540-2.